

Isotopic and Chemical Titration of Acid Sites in Tungsten Oxide Domains Supported on Zirconia

Chelsey D. Baertsch, Stuart L. Soled,[†] and Enrique Iglesia*

Department of Chemical Engineering, University of California at Berkeley, Berkeley, California 94720, and Corporate Strategic Research Lab, ExxonMobil Research and Engineering, Route 22 East, Annandale, New Jersey 08801

Received: August 24, 2000; In Final Form: November 27, 2000

The acid and surface properties of $\text{WO}_x\text{-ZrO}_2$ solid acid catalysts were examined as a function of WO_x surface density. Surface density strongly influences the size and electronic properties of WO_x domains and the rate of acid-catalyzed reactions on these materials. The adsorption and isotopic exchange of acid and redox probe molecules (NH_3 , pyridine, H_2 , and O_2) were used to measure the density and type of active sites in the reducing environments required to achieve high isomerization reaction rates. In this manner, the role of H_2 and of surface density on the formation of Bronsted or Lewis acid sites was determined by combining infrared spectroscopy and desorption measurements using NH_3 titrants. At submonolayer WO_x coverages, the density of Bronsted acid sites increased with increasing WO_x surface density up to $\sim 0.20 \text{ NH}_3/\text{W}$ atom, indicating their presence at the interface between ZrO_2 and polytungstate domains. Above monolayer WO_x coverages, Bronsted acid site densities (per W atom) decreased markedly because of the formation of WO_3 clusters. The addition of H_2 during NH_3 adsorption or desorption increased only slightly the ratio of Bronsted to Lewis acid sites and did not change the total adsorption uptake. H_2 chemisorption uptakes at typical reaction temperature (523 K) showed that the number of H atoms adsorbed on $\text{WO}_x\text{-ZrO}_2$ was negligible at low WO_x surface densities ($< 4 \text{ W/nm}^2$). Hydrogen uptakes increased as reducible polytungstate domains formed with increasing surface density, reaching a maximum value of 0.063 H/W at 7.35 W/nm^2 . H_2 uptakes decreased at higher surface densities because of reduction processes that lead to oxygen removal from WO_x domains, as shown by O_2 chemisorption uptakes on these samples. Oxygen-deficient WO_{3-x} species are unable to stabilize adsorbed hydrogen by delocalizing electron density to form $\text{H}^{\delta+}$. The density of these minority $\text{H}^{\delta+}$ Bronsted acid sites formed during exposure to H_2 , and the rate of *o*-xylene isomerization on $\text{WO}_x\text{-ZrO}_2$, shows a similar dependence on WO_x surface density. These findings suggest that temporary acid sites formed by H_2 dissociation and adsorption on basic oxygens in WO_x domains lead to very active Bronsted acid sites, which catalyze *o*-xylene isomerization with turnover rates much higher than on H-ZSM5. Isotopic exchange of surface OH groups with D_2 , after H_2 pretreatments that lead to chemisorbed hydrogen, confirmed the low density of O–H species formed from H_2 on $\text{WO}_x\text{-ZrO}_2$ (0.017 H atoms/W atom at 7.8 W/nm^2).

Introduction

Acid-catalyzed isomerization and alkylation reactions form hydrocarbon molecules with useful properties as fuels, lubricants, and detergents. The required acid catalysts include toxic and corrosive liquid acids, such as H_2SO_4 and HF, metal halides, and metal oxides promoted with Cl or F. These reagents pose significant risks in handling, containment, disposal, and regeneration. Many solid acids, such as zeolites, complex oxides, and clays, avoid these difficulties, and they are gradually replacing liquids and halogen-containing compounds as acid catalysts in chemical processes.¹ Mesoporous oxides with open pore structures are particularly attractive because they avoid secondary reactions promoted by diffusional constraints that slow down the removal of initial isomerization or alkylation products from catalyst pellets.

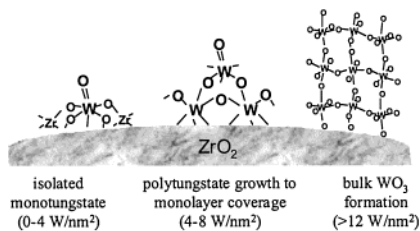
ZrO_2 promoted with sulfate groups ($\text{SO}_x\text{-ZrO}_2$) is a potential replacement for solid acids; it catalyzes alkane isomerization near room temperature.² The initial description of these materials

as superacids, based on this catalytic behavior, has proven to be incorrect. Recent studies have concluded that $\text{SO}_x\text{-ZrO}_2$ and the more active $\text{SO}_x\text{-ZrO}_2$ promoted with Fe or Mn contain acid sites of moderate strength, but the presence of redox sites can initiate low-temperature reactions of alkanes by initially forming the required alkene intermediates.^{3–6} $\text{SO}_x\text{-ZrO}_2$ catalysts deactivate rapidly during many reactions and tend to leach H_2S and SO_x during H_2 and air treatments, respectively, and H_2SO_4 in the presence of H_2O . These processes cause irreversible loss of catalyst activity and also downstream containment and corrosion issues.

WO_x domains supported on ZrO_2 also behave as solid acids, and they are stable at high temperatures in H_2 , O_2 , or H_2O atmospheres. $\text{WO}_x\text{-ZrO}_2$ catalyzes the isomerization of butane at 323 K and of pentane at 303 K after treatment in air at 1073 K, but the selectivity to undesired cracking products is very high ($> 50\%$).⁷ The presence of Pt in $\text{WO}_x\text{-ZrO}_2$ and of H_2 in the reactant stream led to high *n*-heptane isomerization selectivity ($> 90\%$) at 473 K.⁸ *n*-Alkane isomerization rates and selectivities on $\text{SO}_x\text{-ZrO}_2$ were also increased by Pt and H_2 , but the cracking selectivities were significantly higher than on

* To whom correspondence should be addressed. Fax: 510-642-4778. E-mail: iglesias@cchem.berkeley.edu.

[†] ExxonMobil Research and Engineering.

SCHEME 1: Growth of WO_x Domain Size with Increasing WO_x Surface Density


Pt/WO_x-ZrO_2 .⁸ The promoting effect of H_2 in the presence of Pt for SO_x-ZrO_2 and WO_x-ZrO_2 catalysts reflects the role of H adatoms in the desorption of isomerized adsorbed intermediates before undesired β -scission or oligomerization events occur.⁸⁻¹¹ These isomerization pathways differ from the bifunctional mechanisms prevalent at higher temperatures, which involve the intermediate formation of alkenes on Pt sites and their subsequent reaction on Bronsted acid sites. H_2 actually inhibits such pathways by decreasing the equilibrium concentration of the required alkene intermediates.

H_2 also increases rates of cumene cracking on Pt/SO_x-ZrO_2 ¹⁰ and of *o*-xylene isomerization on metal-free WO_x-ZrO_2 .^{12,13} These two reactions can proceed via monofunctional pathways requiring only Bronsted acid sites and no hydrogen transfer steps. These observations would suggest that H_2 increases the density of the required Bronsted acid sites on these materials. H_2 also inhibited deactivation processes during *o*-xylene isomerization on WO_x-ZrO_2 , but the hydrogen effects remained even after extrapolation to zero time on stream.^{12,13} The H_2 effects observed on Pt/SO_x-ZrO_2 led to the proposal that H_2 dissociation forms H adatoms that transform Lewis acid centers into Bronsted acids.¹⁰ This proposal was confirmed by infrared evidence using adsorbed bases as titrants.¹⁴ In this study, we explore similar mechanisms that may account for H_2 effects on monofunctional isomerization reactions catalyzed by metal-free WO_x-ZrO_2 .

The structure and catalytic properties of WO_x-ZrO_2 are influenced markedly by W concentration and thermal treatment. Maximum pentane isomerization rates were observed in samples with 19–24 wt % WO_3 after treatment at 923–1123 K.^{7,15,16} The treatment temperature required for maximum *o*-xylene isomerization rates decreased with increasing W concentration,¹⁷ leading to the proposal that intermediate WO_x surface densities on ZrO_2 led to active sites residing on the surface of two-dimensional polytungstate domains.¹⁸ *o*-Xylene isomerization rates (per W atom) depended only on the WO_x surface density, reaching a maximum value at ~ 10 W/nm^2 , whether this surface density was achieved by varying the W concentration or the treatment temperature.^{17,19}

Raman, UV-visible, and X-ray absorption spectroscopic studies¹⁷⁻¹⁹ showed that the structure and size of WO_x domains in WO_x-ZrO_2 (Scheme 1) also depend only on the WO_x surface density. Isolated monotungstate species are present at low WO_x surface densities (<4 W/nm^2), but they condense into two-dimensional polytungstate domains as the surface density increases to ~ 10 W/nm^2 . These polytungstate species appear to provide the active sites required for *o*-xylene isomerization at 523 K, since isomerization rates are much lower on samples lacking these polytungstate domains (<4 W/nm^2) and isomerization rates increase as the surface density increases up to monolayer WO_x values. Higher surface densities lead to WO_3 clusters with lower surface area and much lower reaction rates. X-ray absorption near-edge spectra showed that WO_x structures

TABLE 1: Catalyst Properties and Nomenclature

W loading (wt % WO_3)	treatment temp (K)	surface area (m^2/g)	surface density (W/nm^2)	nomenclature
3	873	93	0.8	WZ-0.8
9	973	65	3.6	WZ-3.6
9	1073	48	4.9	WZ-4.9
10	1073	52	5.0	Pt/WZ-5.0
12	1073	51	6.1	WZ-6.1
12	1123	40	7.8	WZ-7.8
12	1143	35	8.9	WZ-8.9
15	1073	39	10.1	WZ-10.1
20	1098	43	12.1	WZ-12.1
30	933	81	9.6	WZ-9.6
30	973	73	10.7	WZ-10.7
30	1073	44	17.7	WZ-17.7
0	773	125		ZrO_2
100				WO_3

retain the distorted octahedral structure of bulk WO_3 at all surface densities.¹⁷⁻¹⁹ Therefore, the marked changes in catalytic rates observed between 0 and 20 W/nm^2 do not reflect changes in local W coordination; rather, they reflect changes in the size of the WO_x domains in which W atoms exist. This study contributes some evidence toward a previous proposal^{13,19} addressing the effects of H_2 and domain size on catalytic behavior by determining the density and nature of the active sites in WO_x-ZrO_2 . In the process, we also provide confirmatory evidence for previously reported claims of a very low density of active sites on these materials.¹⁵ The adsorptive and redox properties were studied using NH_3 , O_2 , and H_2 as titrants as a function of WO_x surface density and of the reductive or oxidative environment or pretreatment.

Experimental Methods

Catalyst Preparation. WO_x-ZrO_2 was prepared by methods previously reported.^{7,8} High surface area zirconia oxyhydroxide ($ZrO_x(OH)_{4-2x}$) was precipitated from a 0.5 M zirconyl chloride solution ($ZrOCl_2 \cdot 8H_2O$, Aldrich, >98 wt %) at a constant pH of 10 using NH_4OH . The precipitate was filtered and washed in order to remove Cl^- and then dried at 383 K. $ZrO_x(OH)_{4-2x}$ was impregnated to incipient wetness with an ammonium metatungstate solution ($(NH_4)_6H_2W_{12}O_{40}$, Strem Chemicals, 99.9%) and then treated in dry air at 773–1273 K. Pt/WO_x-ZrO_2 (0.3 wt. % Pt) was prepared by impregnation of WO_x-ZrO_2 (10 wt % WO_3 , treated in air at 1073 K) with a solution of $(NH_3)_4Pt(OH)_2$, dried at 383 K, and then treated in air at 723 K.

WO_x surface density was varied by changing the tungsten concentration and the treatment temperature.¹⁹ WO_x-ZrO_2 samples with 3–30 wt % WO_3 were treated in flowing dry air (Matheson, zero grade, 0.50 cm^3 s^{-1}) at 773–1098 K in order to obtain samples with WO_x surface densities between 0.8 and 17.7 W/nm^2 . Pure ZrO_2 was prepared by treating $ZrO_x(OH)_{4-2x}$ in dry air at 773 K in order to preserve the high surface area tetragonal phase prevalent at all treatment temperatures in WO_x-ZrO_2 samples. Bulk WO_3 powder was obtained from Aldrich (99.9%). All samples used in NH_3 adsorption-desorption, infrared, and D_2-OH studies are described in Table 1. These samples will be referenced by their WO_x surface density throughout because their structure and catalytic properties depend only on their surface density.

Chemisorption and Physisorption. H_2 , O_2 , and CO_2 chemisorption uptakes were measured using a Quantachrome 1C Autosorb apparatus. Samples were dehydrated in He at 673 K for 4 h and then evacuated at 313 K before measuring CO_2 uptakes between 2.7 and 53 kPa at 313 K. Saturation coverages

of strongly adsorbed CO₂ were calculated by extrapolating these isotherms to zero pressure in order to subtract physisorbed CO₂.

A WO_x-ZrO₂ sample (3 g; 30 wt % WO₃) was treated in flowing dry air for 1 h at temperatures between 773 and 1073 K before H₂ or O₂ chemisorption measurements in order to obtain the desired WO_x surface density. These chemisorption experiments required a sequence of steps. The sample was first evacuated at 523 K until the degassing rate was below 0.2 μmol/s; a nine-point H₂ adsorption isotherm at 523 K was then measured between 2.5 and 80 kPa. After these measurements, the sample was treated in flowing H₂ at 523 K for 1 h. It was then evacuated at 523 K until low degassing rates were achieved, and a nine-point O₂ isotherm was measured at 523 K between 2.5 and 80 kPa. H₂ and O₂ uptakes are reported at the highest pressure in this range (80 kPa), because it is closest to the H₂ pressure used in catalytic experiments (100 kPa), and thus an accurate indication of the amount of hydrogen chemisorbed during steady-state reactions. Multipoint BET isotherms were obtained by N₂ physisorption at 77 K using a Quantasorb surface area analyzer after evacuating samples at 473 K for 2 h.

Infrared Spectroscopy. The color of WO_x-ZrO₂ samples changes from light yellow to blue when treated with H₂ at 523 K; these samples absorb and scatter a significant fraction of incident infrared radiation, thus requiring diffuse reflectance infrared methods (DRIFTS). In-situ diffuse reflectance spectra were obtained using a Mattson RS-10000 Fourier transform infrared spectrometer adapted with a diffuse reflectance attachment (Harrick Scientific; DRP-XXX) and in-situ cell (HVC-DR2). A MCT detector cooled by liquid N₂ was used at a resolution of 4 cm⁻¹. Catalyst samples were placed as powders (<0.12 mm particle diameter) on a porous quartz disk through which gases were introduced (0.83 cm³ s⁻¹). WO_x-ZrO₂ samples were dehydrated in flowing dry air (0.83 cm³ s⁻¹) at 773 K for 1 h, purged with flowing Ar (1.67 cm³ s⁻¹) at room temperature for 1 h, and then treated in Ar or H₂ (Matheson, UHP, 0.83 cm³ s⁻¹) at 523 K for 1 h before NH₃ adsorption and infrared measurements. The H₂ treatment at 523 K, used throughout this study, attempts to replicate the conditions used in *o*-xylene reaction studies.^{13,17} NH₃ was adsorbed at 298 K using a flow of 0.93% NH₃ in He (Altair, certified standard, 0.83 cm³ s⁻¹) diluted with either Ar or H₂ (0.83 cm³ s⁻¹). The spectra of adsorbed NH₃ were obtained at temperatures between 298 and 773 K after purging the sample of gaseous or physisorbed NH₃ using H₂ or Ar at 298 K for 1 h.

The spectra of adsorbed NH₃ were recorded in reflectance units (eq 1)

$$\text{reflectance } R = \frac{R_{\text{sample}}}{R_{\text{reference}}} \quad (1)$$

using dehydrated samples before NH₃ adsorption as a reference. The relative reflectivity of the absorber was related to its concentration using apparent absorbance units (eq 2).

$$\text{apparent absorbance } A = -\log(R) \quad (2)$$

The Kubelka-Munk function²⁰ (eq 3)

$$\text{Kubelka-Munk function } f(R) = \frac{(1 - 2R)^2}{2R} \quad (3)$$

was calculated to compare samples after dehydration, using the reflectance of KBr as a reference. Absorption cross sections for NH₃ adsorbed on Bronsted and Lewis acid sites in WO_x-ZrO₂ are not known; thus, the absolute concentration of Bronsted

and Lewis acid sites cannot be quantified by infrared measurements alone. However, the relative number of these two types of sites can be determined for a given sample as a function of temperature or pretreatment, and between samples assuming a constant scattering coefficient.²¹

Temperature-Programmed Desorption. Temperature-programmed desorption (TPD) of preadsorbed NH₃ was carried out after WO_x-ZrO₂ samples (~1 g) were dehydrated at 773 K in dry air (1.67 cm³ s⁻¹) for 1 h, purged with Ar (1.67 cm³ s⁻¹) at room temperature for 0.5 h, and then treated with Ar or H₂ (1.67 cm³ s⁻¹) at 523 K for 1 h. NH₃ was adsorbed by exposing samples treated in this manner to a stream containing 0.93% NH₃ in He (0.83 cm³ s⁻¹) mixed with Ar or H₂ (0.83 cm³ s⁻¹) for 1 h at 298 K. NH₃ was desorbed in Ar flow (0.83 cm³ s⁻¹) by increasing the temperature to 973 at 0.17 K/s and measuring the intensity at 16 amu by mass spectrometry (Leybold-Inficon Transpector H200M).

Catalytic Measurements. *o*-Xylene isomerization was carried out in a recirculating batch reactor at 523 K, 0.67 kPa *o*-xylene (NBS, >99.995%), and 106 kPa H₂ (Mattson, UHP).¹⁷ Reactants and products were analyzed by gas chromatography (Hewlett-Packard 5890 GC, 30 m DB-WAX capillary column, flame ionization detector). Catalyst samples (0.030 g) were treated in flowing air (0.83 cm³ s⁻¹) at 773 K, then reduced in flowing H₂ (0.83 cm³ s⁻¹) at 523 K for 1 h. Reactions were conducted at <2% *o*-xylene conversion per pass. Initial reaction rates were determined from the initial slope of W atom turnovers versus time. Rates were normalized by either the number of W atoms, the BET surface area (nm²), or the total number of adsorbed NH₃ molecules.

D₂-OH Isotopic Exchange. The isotopic exchange of D₂ with surface OH groups was used to measure the number of OH groups and the temperature required for D₂ dissociation steps that limit the D₂-OH exchange rates. WO_x-ZrO₂ samples were dehydrated at 773 K in flowing dry air (1.67 cm³ s⁻¹) for 1 h, cooled to room temperature, purged with flowing Ar at 298 K, and then treated with either Ar or H₂ (1.67 cm³ s⁻¹) at 523 K for 1 h. After cooling to room temperature, samples were exposed to a 5% D₂/Ar mixture (Matheson, certified standard, 1.67 cm³ s⁻¹) and the temperature was increased to 823 K at 0.17 K/s. The evolution or consumption of HD, H₂, and D₂ was monitored by measuring their gas phase concentration using mass spectrometry (Leybold-Inficon Transpector H200M).

Results and Discussion

Infrared Spectroscopy of Dehydrated WO_x-ZrO₂. The spectra for WZ-3.6, WZ-9.6, WZ-17.7, ZrO₂, and bulk crystalline WO₃ in air at 773 K are shown in Figure 1 (W=O stretch region, 1700–2500 cm⁻¹) and Figure 2 (O-H stretch region, 3400–4000 cm⁻¹). Before dehydration, adsorbed water led to a sharp infrared band at 1630 cm⁻¹ and to a broad band at 2600–3600 cm⁻¹, both of which disappeared after treatment at 773 K in dry air. Stretching modes for W=O species at the surface were observed at 2004, 2008, and 2013 cm⁻¹ on WZ-3.6, WZ-9.6, and WZ-17.7, respectively (Figure 1). These infrared bands confirm the predominant presence of dispersed species in these samples, because W=O species exist only at domain or cluster surfaces. The observed shift in frequency with increasing WO_x surface density reflects changes in the WO_x domain size, also detected by Raman and UV-visible methods.¹⁸ The incipient formation of crystalline WO₃ in WZ-17.7 was detected by two infrared bands: a shoulder at ~2056 cm⁻¹ and a broad band at ~1850 cm⁻¹, corresponding to W-O and/or W=O stretching overtones in monoclinic WO₃.^{22,23} Both

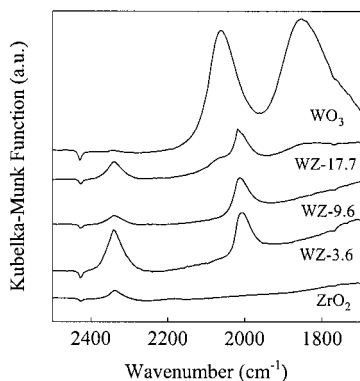


Figure 1. Diffuse reflectance infrared spectra of W–O (1800–2100 cm^{-1}) and Zr–O (2300–2400 cm^{-1}) stretching regions for ZrO_2 , WO_x - ZrO_2 (3.6, 9.6, and 17.7 W/nm^2), and bulk WO_3 after dehydration in dry air at 523 K. Spectra were recorded at 523 K, and the Kubelka–Munk function was calculated using KBr as a reference.

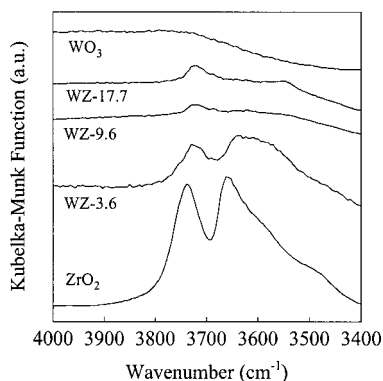


Figure 2. Diffuse reflectance infrared spectra of the O–H stretching region for ZrO_2 , WO_x - ZrO_2 (3.6, 9.6, and 17.7 W/nm^2), and bulk WO_3 after dehydration in dry air at 523 K. Spectra were recorded at 523 K, and the Kubelka–Munk function was calculated using KBr as a reference.

WO_x - ZrO_2 and ZrO_2 show an infrared band at 2333 cm^{-1} , which appears to be an overtone of a low-frequency Zr–O stretch.

Figure 2 shows the effect of WO_x surface density on the stretching frequency of OH groups on ZrO_2 . Pure ZrO_2 shows bands at 3655 and 3735 cm^{-1} , corresponding to tetragonal ZrO_2 .²⁴ The presence of WO_x shifts the band at 3735 cm^{-1} to 3720 cm^{-1} for all WO_x surface densities; it also broadens the band at 3655 cm^{-1} , while gradually shifting it to lower frequencies with increasing WO_x surface density. These frequency shifts reflect interactions between WO_x domains and the ZrO_2 support, possibly as Zr–O–W linkages, which can alter the vibrational properties of vicinal hydroxyl groups. The significant decrease in the intensity of the OH bands for WO_x - ZrO_2 compared to ZrO_2 confirms the anchoring of WO_x species onto Zr oxyhydroxide surfaces during synthesis and pretreatment.

Infrared Spectroscopy of Adsorbed NH_3 . Infrared spectroscopy of adsorbed NH_3 and pyridine was used to investigate the type of acid sites (Bronsted vs Lewis) in WO_x - ZrO_2 samples with varying WO_x surface density and the influence of H_2 on the formation and number of Bronsted acid sites. Only NH_3 adsorption results are presented here, but similar conclusions were reached using pyridine as the titrant. Two frequency regions for adsorbed NH_3 were monitored: N–H stretching modes at 2500–3600 cm^{-1} and N–H deformation modes at 1100–1800 cm^{-1} .

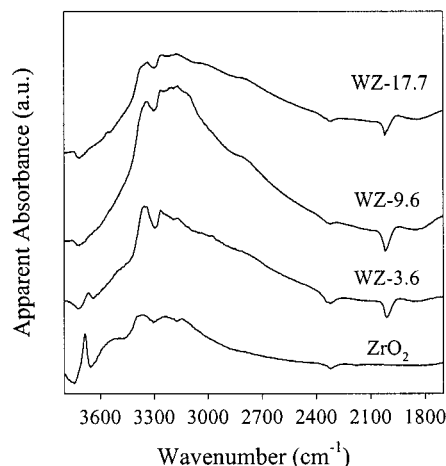


Figure 3. Diffuse reflectance infrared spectra of the N–H stretching region (ν) of NH_3 adsorbed on ZrO_2 and WO_x - ZrO_2 (3.6, 9.6, and 17.7 W/nm^2) at 523 K. NH_3 was adsorbed at 298 K in Ar, then heated to 523 K in Ar to record the spectra. Apparent absorbance units were calculated using the dehydrated samples before NH_3 adsorption as a reference.

Spectra for NH_3 adsorbed on ZrO_2 , WZ-3.6, WZ-9.6, and WZ-17.7 are shown in Figure 3 at 523 K for the N–H stretching frequency range, using the dehydrated WO_x - ZrO_2 spectrum before NH_3 adsorption (shown in Figure 2) as a reference. For the spectra shown in Figure 3, NH_3 was adsorbed at 298 K in Ar and then treated in Ar at 298 K. The temperature was increased to 523 K in flowing Ar, and the spectra were measured. Negative peaks at 2004–2013 cm^{-1} (W=O) and 2333 cm^{-1} (Zr–O) show that NH_3 adsorbs on both ZrO_2 surfaces and WO_x domains. The negative peaks near 3600 and 3700 cm^{-1} show that some adsorbed NH_3 interacts with OH groups as well. Before NH_3 adsorption on ZrO_2 , O–H stretching vibrations were detected at 3655 and 3735 cm^{-1} (Figure 2). The negative bands at 3655 and 3735 cm^{-1} and the appearance of a band near 3680 cm^{-1} after NH_3 adsorption on ZrO_2 show a shift in the frequency of the residual OH groups and a net decrease in their infrared absorption intensity, both arising from interactions of these OH groups with adsorbed NH_3 . Hydrogen bonding between NH_3 and OH groups causes this frequency shift on ZrO_2 , and also on WO_x - ZrO_2 , but the intensity of the residual Zr–OH groups and W–OH species on WO_x - ZrO_2 is much smaller (Figures 2 and 3), especially for samples with WO_x surface densities above monolayer coverage (WZ-9.6 and WZ-17.7). The presence of hydrogen-bonded NH_3 on both WO_x - ZrO_2 and ZrO_2 is evident from the broad N–H deformation bands (2500–3600 cm^{-1}), which are typically associated with extensive hydrogen bonding.²⁵

NH_3 interacts with O–H groups on both ZrO_2 and WO_x - ZrO_2 , but protonated NH_3 is detected only on WO_x - ZrO_2 samples. These protonated species require Bronsted acid sites and lead to infrared bands at 2800–3100 cm^{-1} , while NH_3 molecules coordinated to Lewis acid sites show vibrations at 3100–3400 cm^{-1} .^{26,27} Lewis acid sites were detected on both ZrO_2 (3350, 3320, and 3125 cm^{-1}) and on all WO_x - ZrO_2 samples (3335, 3235, and 3140 cm^{-1}) (Figure 3). Broad absorption bands at 2975 and 2750 cm^{-1} , indicating the presence of Bronsted acid sites, were observed on WZ-3.6, WZ-9.6, and WZ-17.7, but not on ZrO_2 , and they became more intense with increasing WO_x surface density. The formation of Bronsted acid sites on ZrO_2 upon WO_x addition was previously detected using pyridine adsorption in He at 298–723 K²⁸ and CO adsorption at 77 K.¹⁶

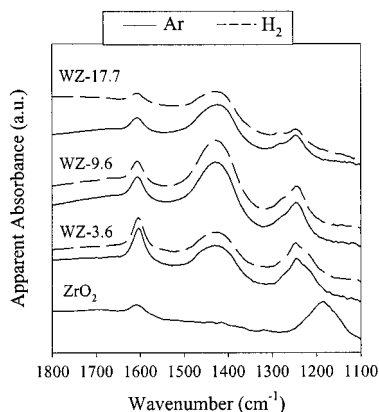


Figure 4. Diffuse reflectance infrared spectra of the N–H deformation (δ) region of NH_3 adsorbed on ZrO_2 and $\text{WO}_x\text{-ZrO}_2$ (3.6, 9.6, and 17.7 W/nm^2) at 523 K. NH_3 was adsorbed at 298 K in either Ar (solid lines) or H_2 (dashed lines) and heated to 523 K in the same gas to record the spectra. Apparent absorbance units were calculated using the dehydrated samples before NH_3 adsorption as a reference.

Figure 4 shows the spectra in the N–H deformation region ($1100\text{--}1800\text{ cm}^{-1}$) at 523 K after NH_3 adsorption at room temperature on ZrO_2 , WZ-3.6, WZ-9.6, and WZ-17.7 samples. NH_3 was adsorbed on $\text{WO}_x\text{-ZrO}_2$ in either inert (Ar) or reducing (H_2) atmospheres at 298 K; the temperature was then increased to 523 K in either Ar or H_2 flow and the spectra were measured. The N–H deformation bands shown in Figure 4 are sharper and more distinct than the N–H stretching bands shown in Figure 3; thus, the relative amounts of Bronsted (B) and Lewis (L) acid sites can be determined more accurately from these N–H deformation bands. Infrared bands at 1180 cm^{-1} (δ_s) and 1603 cm^{-1} (δ_{as}) were detected on pure ZrO_2 ; they were also observed and attributed to NH_3 coordinated to Lewis acid sites in previous studies.²⁹ On $\text{WO}_x\text{-ZrO}_2$ samples, the band at 1180 cm^{-1} (δ_s) for ZrO_2 shifts to higher frequency (1241 cm^{-1}), but it is not influenced by the W surface density on WZ-3.6, WZ-9.6, or WZ-17.7 samples. This symmetric N–H deformation mode appears to be quite sensitive to the identity of the coordinating cation;²⁹ as a result, it can be used as an indicator of Lewis acid strength. The observed shift to higher frequency with the addition of WO_x domains indicates that Lewis acid sites on WO_x species supported on ZrO_2 are significantly stronger than those on ZrO_2 , apparently as a result of the higher electronegativity of W^{6+} compared to Zr^{4+} .^{29,30} NH_3 adsorbed at 523 K on $\text{V}_2\text{O}_5\text{-TiO}_2$ at submonolayer coverages showed a symmetric N–H deformation band at 1230 cm^{-1} ,²⁷ which lies between the bands detected on WO_x and ZrO_2 , as expected from the intermediate oxidation state and electronegativity of the V^{5+} coordinating cations. The WO_x surface density ($3.6\text{--}17.7\text{ W}/\text{nm}^2$) did not influence the frequency of the $\delta_s(\text{N-H})$ band, suggesting that the Lewis acid strength and oxidation state of the W cations are unaffected by domain size; the latter is consistent with previous X-ray absorption spectroscopic studies.¹⁹

In contrast with ZrO_2 , $\text{WO}_x\text{-ZrO}_2$ samples showed a band at 1420 cm^{-1} corresponding to the asymmetric N–H deformation mode (δ_a) in protonated NH_3 (Figure 4).^{26,27,31} A relative measure of the density of Bronsted and Lewis acid sites can be obtained from the areas under the 1420 cm^{-1} (B) and the 1241 cm^{-1} (L) bands. This relative Bronsted/Lewis acid site density ratio, shown for WZ-3.6, WZ-9.6, WZ-17.7, and Pt/WZ-5.0 samples at 523 K in Figure 5, was used to examine the effect of H_2 and of WO_x surface density on the number and type of acid sites in $\text{WO}_x\text{-ZrO}_2$. Figure 5 shows that the ratio of

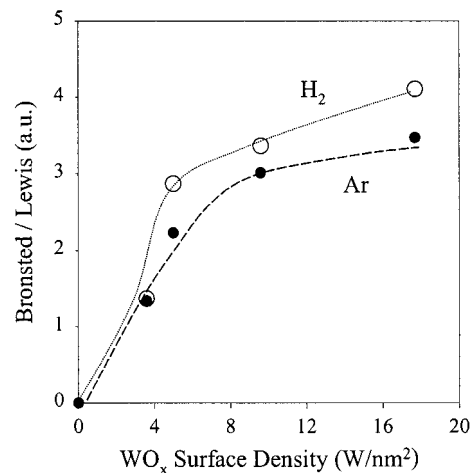


Figure 5. Bronsted/Lewis acid site density ratio at 523 K from NH_3 adsorption in H_2 (open circles) or Ar (closed circles) on $\text{WO}_x\text{-ZrO}_2$ as a function of WO_x surface density ($0\text{--}17.7\text{ W}/\text{nm}^2$). This relative ratio was determined from integration of infrared bands corresponding to NH_3 adsorbed on Bronsted acid sites (1420 cm^{-1}) and Lewis acid sites (1241 cm^{-1}). The sample with $5\text{ W}/\text{nm}^2$ contains 0.3 wt % Pt.

Bronsted to Lewis acid sites initially increases with increasing WO_x surface density up to the theoretical polytungstate monolayer value ($\sim 7\text{ W}/\text{nm}^2$). At higher surface densities, this ratio remains almost constant. The observed increase in the ratio of Bronsted to Lewis acid sites may reflect either an increase in the number of Bronsted acid sites and/or a decrease in the number of Lewis acid sites. In either case, it appears that WO_x clusters introduce Bronsted acid sites, possibly in the form of bronzes (H_xWO_3) or of O–H groups stabilized at Zr–O–W and W–O–W linkages in monotungstate and polytungstate species.

The presence of H_2 (50.7 kPa) during NH_3 adsorption (0.47 kPa) at 523 K led to slightly larger Bronsted/Lewis acid site ratios (Figure 5), except for samples with less than $4\text{ W}/\text{nm}^2$, which do not show any evidence of reduction in H_2 at 523 K by UV–visible methods.¹⁸ Although effects of H_2 on the Bronsted/Lewis acid site ratio are evident, the observed effects of H_2 are small (as also determined using pyridine adsorption at 523 K), which is in contrast to the strong H_2 effects observed on initial *o*-xylene isomerization rates. Pyridine adsorption on $\text{Pt}/\text{SO}_x\text{-ZrO}_2$ was affected much more significantly by the presence of H_2 , which led to the apparent conversion of Lewis acid sites into Bronsted acid sites;¹⁴ these effects were detected only on Pt-containing samples. Pt addition to $\text{WO}_x\text{-ZrO}_2$ (Pt/WZ-5.0, shown in Figure 5), however, did not clearly result in stronger H_2 effects on the ratio of Bronsted to Lewis acid sites than on metal-free $\text{WO}_x\text{-ZrO}_2$. If the role of H_2 is to convert Lewis acid sites into Bronsted acid sites on $\text{WO}_x\text{-ZrO}_2$, as reported previously for $\text{Pt}/\text{SO}_x\text{-ZrO}_2$, the number of Bronsted acid sites formed must be much smaller than the total number of acid sites titrated by NH_3 . Scheithauer et al.^{16,25} examined the acid properties of $\text{WO}_x\text{-ZrO}_2$ catalysts with varying surface structures using low-temperature infrared spectroscopy of adsorbed CO. They reported an increase in the density and strength of Bronsted acid sites with increasing WO_x surface coverage, and proposed an active site resembling a Zr-heteropolytungstate with H^+ as the charge compensating species, a type of structure that would not require the presence of H_2 .

Temperature-Programmed Desorption of Ammonia (NH_3 TPD). The total number of acid sites (Bronsted and Lewis) in $\text{WO}_x\text{-ZrO}_2$ samples ($0\text{--}12.1\text{ W}/\text{nm}^2$) was measured from the amount of NH_3 desorbed as samples were heated from 298 to

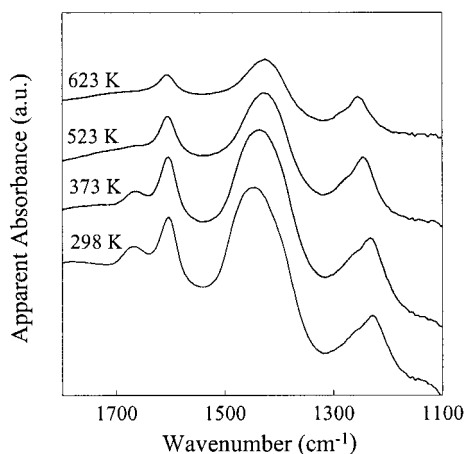


Figure 6. Diffuse reflectance infrared spectra of NH_3 adsorbed in Ar at 298 K on $\text{WO}_x\text{-ZrO}_2$ (9.6 W/nm^2), then desorbed in Ar at increasing temperatures (298, 373, 523, and 623 K), where the spectra were recorded. Apparent absorbance units were calculated using the dehydrated sample before NH_3 adsorption as a reference.

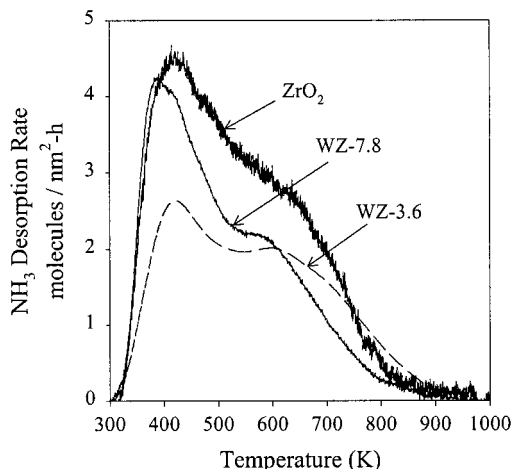


Figure 7. Temperature-programmed desorption profiles for NH_3 adsorbed in Ar at 298 K on ZrO_2 and $\text{WO}_x\text{-ZrO}_2$ (3.6 and 7.8 W/nm^2).

900 K after NH_3 adsorption at 298 K. NH_3 desorption rates for WZ-3.6, WZ-7.8, and ZrO_2 are shown in Figure 7 as a function of desorption temperature. All $\text{WO}_x\text{-ZrO}_2$ samples, which contain both Bronsted and Lewis acid sites, and pure ZrO_2 , which contains only Lewis acid sites and nonacidic OH groups, gave similar desorption profiles. These profiles showed a low-temperature desorption peak centered at $\sim 423 \text{ K}$, and a series of overlapping peaks between 500 and 800 K. Similar NH_3 TPD profiles were reported previously for tetragonal and monoclinic ZrO_2 mixtures,³² $\text{WO}_3/\text{Al}_2\text{O}_3$,³³ Y-zeolite,³³ and $\text{WO}_x\text{-ZrO}_2$.³⁴

NH_3 desorption peaks can be qualitatively assigned to various types of Bronsted and Lewis acid sites by considering these TPD data in concert with NH_3 infrared spectra obtained at various temperatures. Figure 6 shows the spectra for NH_3 adsorbed from an NH_3/Ar stream at 298 K on WZ-9.6, and desorbed in pure Ar between 298 and 623 K. At 298 K, the absorption bands at 1222 cm^{-1} (δ_s) and 1598 cm^{-1} (δ_{as}) correspond to NH_3 coordinated to Lewis (L) acid sites, and the bands at 1439 cm^{-1} (δ_a) and 1661 cm^{-1} (δ_s) to NH_4^+ on Bronsted (B) acid sites.^{26,27,31} A weak shoulder near 1120 cm^{-1} (δ_s) at 298 K reflects traces of hydrogen-bonded or physisorbed NH_3 ,³¹ but this feature disappears at $\sim 373 \text{ K}$. NH_3 adsorbed on Bronsted acid sites appears to be bound less strongly than on Lewis acid sites, since bands associated with protonated NH_3 decrease, or even disappear, at lower temperatures than the

TABLE 2: Total Number of NH_3 Molecules Desorbed per nm^2 of Catalyst Surface Area from 298 to 1173 K (Not Yet Corrected with CO_2 Uptakes for ZrO_2 Surface Area)

catalyst	surface coverage (NH_3/nm^2)	catalyst	surface coverage (NH_3/nm^2)
ZrO_2	2.14	WZ-7.8	1.67
WZ-0.8	1.84	WZ-8.9	1.73
WZ-3.6	1.37	WZ-10.7	1.81
WZ-6.1	1.88	WZ-12.1	1.90

infrared bands for coordinated NH_3 . In general, low-temperature desorption peaks reflect the evolution of physisorbed and hydrogen-bonded NH_3 or of weakly held protonated NH_3 on $\text{WO}_x\text{-ZrO}_2$. The higher temperature desorption peaks correspond to the desorption of NH_3 coordinated to Lewis acid sites and of strongly held NH_3 protonated on Bronsted acid sites in $\text{WO}_x\text{-ZrO}_2$. No significant changes in acid strength between $\text{WO}_x\text{-ZrO}_2$ and ZrO_2 were evident from NH_3 desorption profiles, though infrared spectra showed slight shifts in the $\delta_s(\text{N-H})$ band of coordinated NH_3 , consistent with small changes in Lewis acid strength. Changes in WO_x surface coverage neither influenced NH_3 desorption profiles nor the position of the $\delta_s(\text{N-H})$ infrared band.

The total amount of NH_3 desorbed during TPD from various $\text{WO}_x\text{-ZrO}_2$ samples (Ar pretreated, $0.8\text{--}12.1 \text{ W/nm}^2$, average value for two runs on WZ-3.6) and from pure ZrO_2 are reported in Table 2. NH_3 adsorbs on WO_x domains, but also on ZrO_2 ; therefore, NH_3 uptakes on $\text{WO}_x\text{-ZrO}_2$ samples must be corrected for the amount adsorbed on the ZrO_2 surface in order to extract the number of acid sites associated with WO_x domains. In order to do this, the fraction of the ZrO_2 surface that remains exposed after anchoring WO_x species must be measured. Because CO_2 chemisorbs selectively on ZrO_2 basic sites, but not on WO_x domains,³⁵ CO_2 chemisorption uptakes were used to determine the exposed ZrO_2 surface in $\text{WO}_x\text{-ZrO}_2$ samples.¹⁸ From these data, and the reasonable assumption that the adsorptive properties of the exposed tetragonal ZrO_2 are similar in pure ZrO_2 and in $\text{WO}_x\text{-ZrO}_2$, NH_3 uptakes on WO_x domains were estimated.

CO_2 uptakes and corrected NH_3 uptakes after either H_2 or Ar pretreatments are shown in Figures 8a-c. CO_2 uptakes (per surface area) decreased and NH_3 uptakes (per surface area) increased with increasing WO_x surface density up to the monotungstate saturation coverage ($\sim 4 \text{ W/nm}^2$, from Raman and UV-visible spectra).¹⁸ The linear change in exposed ZrO_2 observed with increasing surface density at low WO_x coverages confirms the initial uniform deposition of well-dispersed monotungstate species throughout ZrO_2 surfaces. At higher WO_x surface densities, the surface becomes saturated with WO_x species and the CO_2 uptakes are small ($< 5\%$ coverage). Also, the areal densities of adsorbed NH_3 reach constant values as the WO_x surface density increases, indicating that two-dimensional polytungstate structures and three-dimensional WO_3 domains possess similar acid site densities (per surface area), despite significant differences in their catalytic and redox properties.^{18,19} The acid site density per W atom (Figure 8c) decreased monotonically with increasing surface density as WO_x species become less accessible to NH_3 , because of the growth of WO_3 domains with internal W atoms. H_2 does not appear to influence NH_3 uptakes on WO_x domains, but any conversion of Lewis into Bronsted acid sites by H_2 would not change the total number of acid sites titrated by NH_3 .

The NH_3 desorption and infrared evidence for the density and type of acid sites were combined to estimate the individual density of Bronsted acid sites on samples with varying WO_x

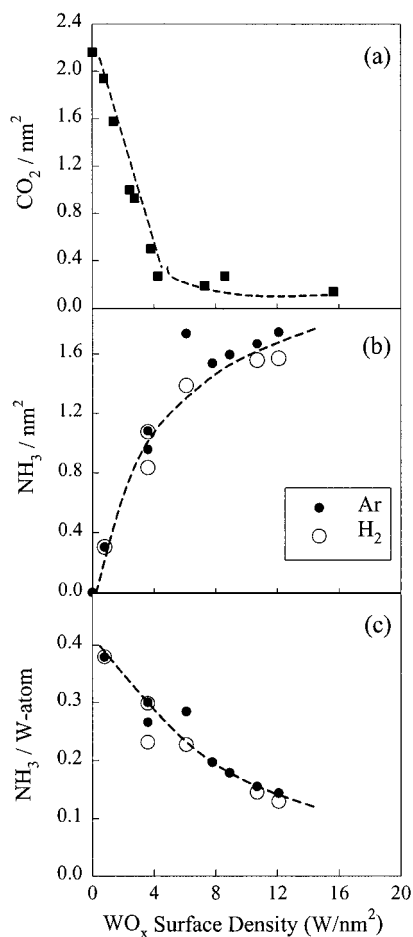


Figure 8. CO_2 uptakes (a) and total WO_x acid site densities [per nm^2 of BET surface area (b) and per W atom (c)] as a function of WO_x surface density. Total acid site densities were calculated from integrated NH_3 desorption (298–900 K) profiles; they were corrected for the NH_3 uptake on ZrO_2 surfaces using CO_2 uptakes. Samples were pretreated at 523 K, and NH_3 was adsorbed at 298 K in either Ar (solid circles) or H_2 (open circles) flow before desorption in Ar. CO_2 uptakes in (a) were adapted from ref 18.

domain size. This estimate required the assumption that the infrared cross sections for NH_3 adsorbed on Bronsted acid sites and on Lewis acid sites are similar. Then, the Bronsted/Lewis acid site density ratios (presented in Figure 5) become concentration ratios. This assumption is reasonable for many solid inorganic oxides,³⁶ and it is, in any case, sufficient to determine relative changes between samples. Total acid site densities (NH_3/nm^2) for WZ-3.6, WZ-9.6, WZ-17.7, and PtWZ-5.0 were estimated by interpolation of the data presented in Figure 8b and combined with the B/L site density ratios shown in Figure 5, without separate analysis of the H_2 -treated vs Ar-treated samples, because the observed differences lie within the error of these estimates.

The fraction of Bronsted acid sites among those titrated by NH_3 is shown in Figure 9a. Most acid sites are of the Bronsted type on $\text{WO}_x\text{-ZrO}_2$ at all WO_x coverages (>50% Bronsted for 3.6–17.7 W/nm^2). Figures 9b and 9c show the estimated number of Bronsted and Lewis acid sites per (BET) surface area and per W atom, respectively. The density of Lewis acid sites per nm^2 of surface area (Figure 9b) remained low and constant for all WO_x surface densities, while the Lewis acid site density per W atom (Figure 9c) decreased with increasing WO_x surface density. Therefore, similar W^{6+} Lewis acid sites are present on all WO_x domains, irrespective of size; yet, W^{6+} centers become less accessible at higher surface coverages because of WO_3

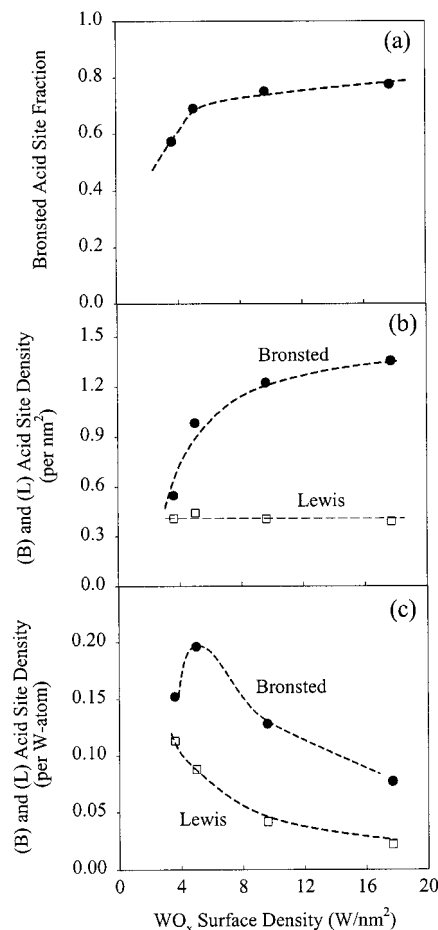


Figure 9. Fraction of acid sites of the Bronsted type (a) and Bronsted and Lewis acid site densities [per nm^2 of BET surface area (b) and per W atom (c)] as a function of WO_x surface density. Bronsted (B) and Lewis (L) acid site densities were calculated by combining NH_3 infrared spectra and TPD measurements.

domain growth. Figure 9b shows that the areal density of Bronsted acid sites increases with increasing WO_x surface density. This trend suggests that Bronsted acid sites on polytungstate domains, which form above monolayer WO_x coverages (>7 W/nm^2), include OH groups associated with W–O–W linkages in addition to those associated with Zr–O–W linkages present on monotungstate species at lower WO_x surface densities. The Bronsted acid site density, per W atom (Figure 9c), appears to increase slightly at submonolayer coverages as bridging W–O–W linkages form in polytungstate domains. At higher surface densities, this Bronsted acid site density (per W atom) decreases because the total number of acid sites (per W atom) on $\text{WO}_x\text{-ZrO}_2$ decreases markedly as three-dimensional WO_3 domains with inaccessible W centers form (see Figure 8c).

o-Xylene isomerization rates, normalized by the number of W atoms or by the total (BET) surface area, show a sharp maximum at intermediate WO_x surface densities.^{17,19} Figure 10 shows initial isomerization rates normalized by the total number of acid sites obtained from the corrected NH_3 uptakes shown in Figure 8b. A similar curve would be obtained for rates normalized by the Bronsted acid site density (Figure 9b). Clearly, NH_3 is not a selective titrant for the active sites specifically responsible for *o*-xylene conversion, because the observed changes in acid site density or strength cannot account for the marked effects of WO_x surface density on isomerization rates. Also, H_2 does not strongly influence either the density or

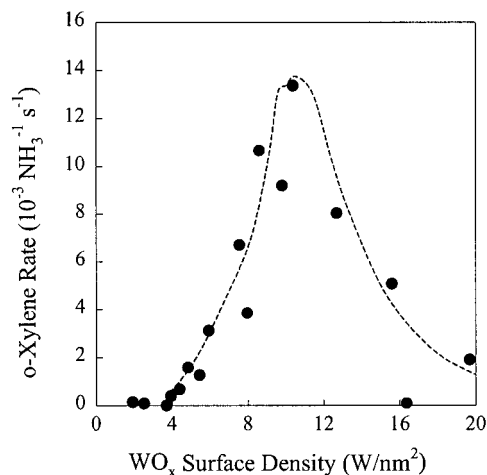


Figure 10. Initial *o*-xylene isomerization rates, normalized by the total Bronsted and Lewis acid site density (determined from NH_3 desorption), as a function of WO_x surface density. Data were adapted from ref 17 using NH_3 uptakes in Figure 8b.

strength of Bronsted acid sites titrated by NH_3 in $\text{WO}_x\text{-ZrO}_2$, even though it has a strong effect on initial xylene isomerization rates. Previous work by Santiesteban et al. showed that the Bronsted acid sites required for *n*-pentane isomerization on $\text{WO}_x\text{-ZrO}_2$ at 483 K were titrated by very small amounts of 2,6-dimethylpyridine (0.0024 strong H^+/W atom, 0.011 total H^+/W atom), and that this acid site density correlated with isomerization turnover rates.¹⁵ Therefore, a more chemically specific molecule that directly probes the active Bronsted acid sites in $\text{WO}_x\text{-ZrO}_2$, which are possibly formed in situ via redox mechanisms, is required. We have chosen H_2 and O_2 for this purpose, because H_2 is required to form active sites during *o*-xylene isomerization and O_2 is a selective poison for these active sites.¹²

H_2 and O_2 Chemisorption. The density and rate of formation of adsorbed hydrogen atoms were measured using H_2 and O_2 chemisorption measurements at 523 K in order to probe their potential presence on the surface during reactions of *o*-xylene/ H_2 mixtures at similar temperatures. H_2 uptakes on a 30 wt % $\text{WO}_x\text{-ZrO}_2$ sample treated in air in the chemisorption cell at temperatures between 773 and 1073 K are shown in Figure 11 as a function of WO_x surface density (closed circles, 4.6–17.7 W/nm^2). H_2 uptakes (H_2/W ratio) reached a maximum value at WO_x surface densities ($\sim 8 \text{ W}/\text{nm}^2$) similar to those required for maximum *o*-xylene isomerization rates (Figure 10), suggesting that active sites may contain adsorbed hydrogen species formed during catalytic reactions by H_2 dissociation. A possible mechanism for the formation of Bronsted acid sites is shown in Scheme 2. It involves the dissociation of H_2 and the migration of H adatoms to WO_x domains, which stabilize protons ($\text{H}^{\delta+}$) by delocalizing the compensating electron density among several W^{6+} Lewis acid centers (the role of the ZrO_2 support will be discussed later). The required delocalization is not available on isolated monotungstate species, because of their large band gap and small domain size compared with polytungstate domains and WO_3 clusters; as a result, H_2 chemisorption uptakes are very low on $\text{WO}_x\text{-ZrO}_2$ samples with low surface density (Figure 11).

These findings are consistent with the difficult reduction of samples with low WO_x surface density detected by UV–visible methods.¹⁸ Hydrogen uptakes increased as polytungstate domains formed, because of their ability to delocalize electron density over several WO_x moieties. Again, the greater tendency of these larger domains to adsorb hydrogen is consistent with

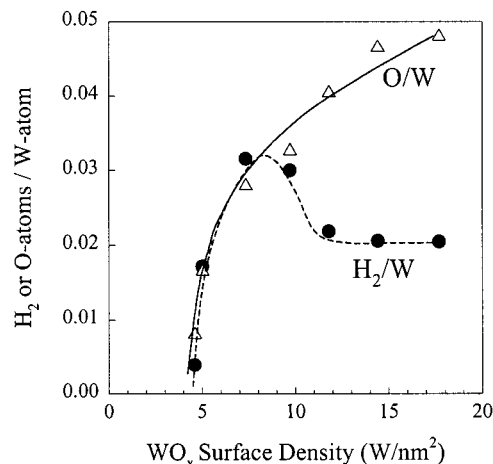


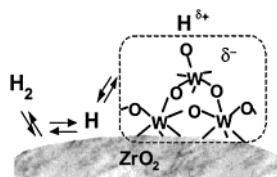
Figure 11. H_2 (closed circles, H_2/W) and O_2 (open triangles, O/W) chemisorption uptakes at 523 K and 80 kPa (H_2 or O_2) as a function of WO_x surface density. H_2 uptakes were obtained after calcination in air at 773–1073 K, and O_2 uptakes were obtained after H_2 reduction at 523 K.

the higher formation rate and the higher density of $\text{W}^{(6-\delta)+}$ color centers detected by UV–visible studies during treatment in H_2 at 523 K.¹⁸ The ability of these larger domains to delocalize electron density is also evident from the decrease in the UV–visible edge energy with increasing WO_x surface density.^{18,25}

As the WO_x surface density increases above monolayer coverages, Raman, UV–visible, and ultimately X-ray diffraction detect the formation of three-dimensional WO_3 crystallites.^{18,19,25,34} These WO_3 crystallites can adsorb hydrogen, but they can also form oxygen-deficient WO_{3-x} (with the concurrent formation of H_2O) and tungsten bronzes with inaccessible hydrogens (H_xWO_3). The formation of H_2O during volumetric chemisorption measurements can mimic the chemisorption of H_2 if it remains adsorbed, but it is undetectable if each H_2O desorbs and replaces one H_2 in the gas phase. During dehydration of $\text{WO}_x\text{-ZrO}_2$ in air, infrared bands corresponding to adsorbed water were detected up to 673 K; thus, it appears likely that any H_2O formed during contact with H_2 at 523 K will remain adsorbed. As $\text{WO}_x\text{-ZrO}_2$ samples reached surface densities slightly above the polytungstate monolayer values ($\sim 7 \text{ W}/\text{nm}^2$), H_2 uptakes initially decreased, apparently as a result of the formation of WO_{3-x} species (Figure 11). These oxygen-deficient species would have higher electron densities than a stoichiometric WO_3 domain, and they are less likely to accommodate the additional negative charge required to form $\text{H}^{\delta+}$ species. H_2 uptakes reached a constant value for WO_x surface densities above 12 W/nm^2 , apparently because of the formation of bulk H_xWO_3 and WO_{3-x} species with a constant stoichiometry.

O_2 uptakes on samples reduced in H_2 at 523 K are also shown in Figure 11 (open triangles, O/W ratio). Unlike H_2 uptakes, O_2 uptakes increased monotonically with increasing WO_x surface density. The O/H_2 stoichiometry is unity up to about 8 W/nm^2 ; this is the expected value if adsorbed hydrogen species formed during contact with H_2 at 523 K react to form adsorbed water during O_2 adsorption measurements. At higher WO_x surface densities, the O/H_2 stoichiometry becomes greater than 1, indicating that O_2 is also required in order to replace the oxygen atoms removed during the H_2 treatment that formed WO_{3-x} species. Therefore, the lower activity of $\text{WO}_x\text{-ZrO}_2$ samples with WO_x surface densities above monolayer values may reflect a combination of several factors that become important as three-dimensional WO_3 structures grow: (1) loss of dispersion; (2)

SCHEME 2: Mechanism for the Formation of Bronsted Acid Sites from H₂ on WO_x-ZrO₂ via the Partial Reduction of W⁶⁺ Lewis Acid Centers in Polytungstate Domains, Which Can Delocalize the Accommodating Negative Charge



formation of bulk H_xWO₃ species with inaccessible hydrogens; and (3) formation of WO_{3-x} species that do not adsorb hydrogen or form bronzes in the presence of H₂.

The *o*-xylene isomerization rate on a WO_x-ZrO₂ sample (8.4 W/nm²), normalized by the number of H^{δ+} Bronsted acid sites or H atoms adsorbed at 523 K, was compared with *o*-xylene turnover rates (per Al atom or H^{δ+}) on H-ZSM5 at identical conditions.¹³ Turnover rates are about 15 times greater on WO_x-ZrO₂ than on H-ZSM5. Although the active Bronsted acid site density in WO_x-ZrO₂ catalysts is very low, reaching a maximum value of only 0.063 H/W for WO_x-ZrO₂ samples with 7.2 W/nm² (Figure 11), it appears that these H^{δ+} species formed via redox processed during the catalytic reaction are extremely active. Even lower densities of Bronsted acid sites were reported in a previous study (0.011 H⁺/W for WO_x-ZrO₂ with 7.9 W/nm²).¹⁵ These conclusions were reached by measuring the number of 2,6-dimethylpyridine molecules required to decrease *n*-pentane isomerization rates at 483 K, after extensive treatment of the sample to ensure homogeneous dispersion of the titrant only on active sites. This titrant selectively interacts with Bronsted acid sites because the sterically hindered N atom is unable to coordinate to Lewis centers.

The number of Bronsted acid sites formed by H₂ chemisorption and apparently responsible for high *o*-xylene turnover rates is significantly less than the total number of acid sites titrated by NH₃ on WO_x domains (Figures 8c and 11, ~3 adsorbed NH₃ per chemisorbed H atom at 7.5 W/nm²). As a result, the permanent but catalytically inefficient acidity provided by W-O-Zr linkages and probed by NH₃ and pyridine adsorption is a poor indicator of catalytic performance. The redox properties of the WO_x domains and their ability to stabilize chemisorbed hydrogen during exposure to H₂ at typical reaction temperatures provide a much more accurate measure of the unique catalytic properties of these materials.

D₂-OH Isotopic Exchange. The isotopic exchange of surface OH species with D₂ to form HD(g) was measured on WO_x-ZrO₂ samples in order to determine the density of OH groups and the rate of D₂ dissociation as a function of WO_x surface density and of pre-reduction treatment. Figure 12 shows the rates of formation of HD on ZrO₂, WZ-3.6, WZ-4.9, WZ-7.8, WZ-10.1, and WZ-12.1 samples treated in H₂ at 523 K before exchange. Figure 13 shows the corresponding data for samples treated in Ar before D₂-OH exchange. Total OH surface densities (per nm² BET surface area), obtained by integration of the exchange curves in Figures 12 and 13, are shown in Figure 14 as a function of WO_x surface density after each pretreatment protocol (Ar or H₂). Because of the very low total OH density, data for WO_x-ZrO₂ samples were measured several times and averaged in order to increase the accuracy of the values reported in Figure 14. At low surface densities, WO_x species adsorb hydrogen atoms without removal of oxygen as H₂O, but oxygen removal begins to occur on WO_x-ZrO₂

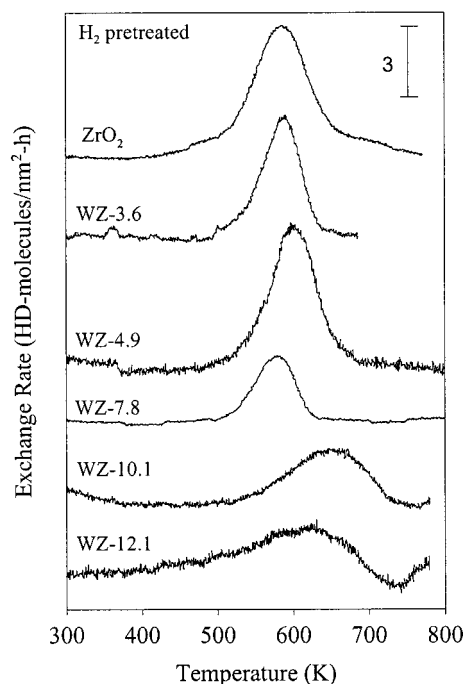


Figure 12. HD evolution rates (HD molecules/(nm² h)), resulting from exchange of OH groups with D₂ on ZrO₂ and WO_x-ZrO₂ (3.6, 4.9, 7.8, 10.1, and 12.1 W/nm²) as a function of temperature. Samples were pretreated in H₂ at 523 K before exchange with D₂.

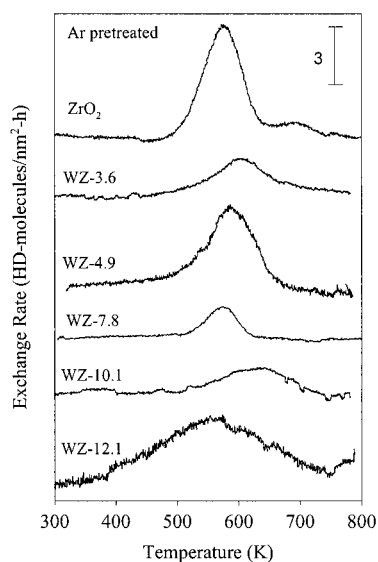


Figure 13. HD evolution rates (HD/(nm² h)), resulting from exchange of OH groups with D₂ on ZrO₂ and WO_x-ZrO₂ (3.6, 4.9, 7.8, 10.1, and 12.1 W/nm²) as a function of temperature. Samples were pretreated in Ar at 523 K prior to exchange with D₂.

samples that exceed the polytungstate monolayer value (as shown by the O₂ chemisorption uptakes required to reoxidize H₂ reduced samples; Figure 11). This overreduction can be detected in the exchange curves for WZ-10.1 and WZ-12.1 shown in Figures 12 and 13, for which negative peaks are observed above 700 K because of the consumption of HD (and D₂) in the reduction of WO₃ to WO_{3-x} with the concurrent formation of water. The consumption of HD (and D₂) on these two samples occurs before D₂ exchange with OH is complete. As a result, the measured OH site densities for the WZ-10.1 and WZ-12.1 samples represent lower than actual values, and the effects of pretreatment on the hydroxyl density are corrupted by this concurrent reduction process.

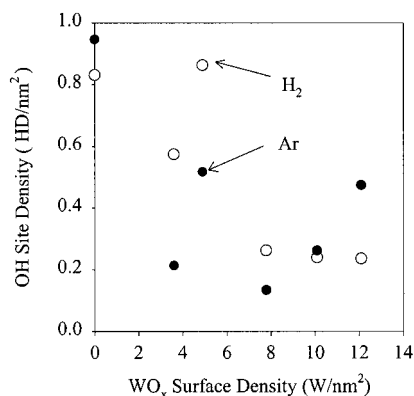


Figure 14. OH site density, determined from the isotopic exchange of OH groups with D_2 , as a function of WO_x surface density. Samples were pretreated at 523 K, before exchange with D_2 , with either H_2 (open circles) or Ar (closed circles).

Samples treated in Ar contain OH groups on exposed ZrO_2 surfaces ($Zr-OH-Zr$) and at the periphery and surface of WO_x domains ($Zr-OH-W$, $W-OH-W$), all of which exchange with D_2 to form HD. Samples pretreated in H_2 at 523 K before exchange can also contain any $H^{\delta+}$ species formed from H_2 dissociation during pretreatment; these species can also exchange with D_2 and contribute to the observed amount of HD formed. Figure 14 shows that H_2 pretreatment can increase the OH site density when WO_x domains are present and able to stabilize the resulting protons and electrons. The apparent density of Bronsted acid sites formed from H_2 can be estimated from the difference in the amount of HD evolved between samples treated in H_2 and in Ar (Figure 14). The density of exchangeable OH groups is higher on ZrO_2 (0.95 OH/nm^2) than on any Ar-treated WO_x-ZrO_2 samples ($<0.52 \text{ H/nm}^2$); thus, it appears that many HD molecules are formed by exchange with nonacidic OH groups on ZrO_2 , the density of which is highest at low WO_x surface coverages. The predominant contribution of ZrO_2 hydroxyls at low WO_x surface densities, and the interference from reduction at high WO_x surface densities, make accurate measurements of the number of OH groups formed by the H_2 treatment difficult. Samples with intermediate surface densities (e.g., WZ-7.8) appear to be influenced least by these two effects. The density of OH groups formed from H_2 on WZ-7.8 was measured to be $0.16 \text{ H atoms/nm}^2$ ($0.020 \text{ H atoms/W atom}$) with this isotopic exchange method, which is a factor of 10 lower than those determined from NH_3 TPD measurements ($0.20 \text{ NH}_3 \text{ molecules/W atom}$ at 7.8 W/nm^2), and almost a factor of 4 lower than the values obtained by H_2 chemisorption measurements ($0.063 \text{ H atoms/W atom}$ at 7.4 W/nm^2).

D_2 -OH exchange requires the dissociation of D_2 and the subsequent exchange of mobile D atoms with surface OH groups. HD evolution rates depend on the D_2 dissociation rate, and thus the gas phase D_2 concentration, as well as on the probability that the resulting mobile D atoms will exchange with OH groups (rather than unproductively with OD groups). This probability in turn depends on the fraction of unexchanged OH groups remaining on the surface. Therefore, HD evolution rates were described using eq 4, in which β is the heating rate. The kinetic parameters (E_a and A) and the remaining OH site density were determined by integrating eq 4 (eq 5), assuming a constant concentration of D_2 in the gas phase and using least-squares estimation methods with HD evolution rates on the low-temperature side of the exchange peaks.

$$R_{HD} = \frac{-d[OH]}{dT} = \frac{A}{\beta} e^{(-E_a/RT)} [OH][D_2] \quad (4)$$

$$\int_{T_0}^T \frac{-d[OH]}{[OH]} = \frac{A[D_2]}{\beta} \int_{T_0}^T e^{(-E_a/RT)} dT \quad (5)$$

The exchange curves predicted by this model for H_2 -pretreated ZrO_2 , WZ-3.6, WZ-4.9, and WZ-7.8 are shown in Figure 15 along with the experimental data. HD exchange rates on submonolayer WO_x-ZrO_2 are accurately described by this first-order process (Figure 15). Isotopic exchange on high WO_x surface density samples (e.g. WZ-10.1 and WZ-12.1), however, deviated from first-order kinetics because exchange processes occurred above 700 K concurrently with WO_x reduction. HD exchange on ZrO_2 can be described by the assumed first-order process (Figure 15), in spite of shoulders present at 475 and 700 K. The low-temperature shoulder is likely due to the presence of minority monoclinic ZrO_2 sites. In fact, we found that the maximum D_2 -OH exchange rate for monoclinic ZrO_2 ($ZrO_x(OH)_{4-2x}$ calcined at 1023 K, $\sim 90 \text{ vol } \% \text{ monoclinic phase}$, not shown) occurs at $\sim 40^\circ \text{C}$ lower temperature than for tetragonal ZrO_2 ($ZrO_x(OH)_{4-2x}$ calcined at 773 K, shown in Figure 15). The high-temperature shoulder at 700 K is possibly due to OH sites present inside the ZrO_2 crystallite, for which exchange would be limited by bulk diffusion.

Kinetic parameters for D_2 -OH exchange on ZrO_2 and WO_x-ZrO_2 are listed in Table 3 (after both H_2 and Ar pretreatments). Activation energies for ZrO_2 , WZ-3.6, and WZ-4.9 are similar ($79-90 \text{ kJ/mol}$). The relatively similar E_a values on ZrO_2 and on low surface density WO_x-ZrO_2 samples, which have significant exposed ZrO_2 surface areas (see Figure 8a), suggest that exposed ZrO_2 surfaces act as D_2 dissociation sites on these WO_x-ZrO_2 samples. Also, E_a values for these samples pretreated in Ar prior to exchange cannot be distinguished (within

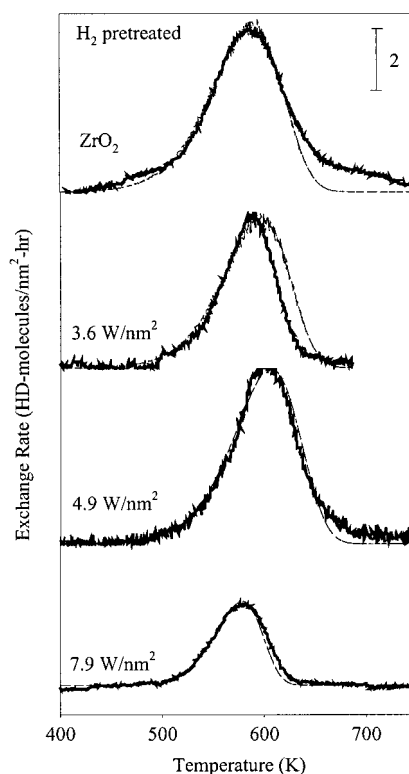


Figure 15. Experimental HD evolution rates (thick solid lines, from Figure 12) and simulated first-order rates (thin dashed lines) for ZrO_2 and WO_x-ZrO_2 (3.6, 4.9, and 7.9 W/nm^2) as a function of temperature.

TABLE 3: First-Order Activation Energies and Rate Constants (at 523 K) for D₂-OH Exchange on ZrO₂ and WO_x-ZrO₂ (3.6–7.8 W/nm²)

catalyst	H ₂ pretreated		Ar pretreated	
	activation energy <i>E_a</i> (kJ/mol)	rate constant <i>k</i> (10 ⁻⁴ s ⁻¹)	activation energy <i>E_a</i> (kJ/mol)	rate constant <i>k</i> (10 ⁻⁴ s ⁻¹)
ZrO ₂	79	5.7	79	7.4
WZ-3.6	88	3.9	90	2.5
WZ-4.9	90	2.8	81	4.9
WZ-7.8	118	5.0	126	5.7

experimental error) from those reduced at 523 K in H₂ before exchange. This is consistent with the presence of H₂ dissociation sites on ZrO₂ surfaces, because ZrO₂ sites are not affected by these reductive treatments, unlike easily reducible WO_x domains. The *E_a* value for WZ-7.8 is measurably larger than for ZrO₂, WZ-3.6, and WZ-4.9 (118–126 vs 79–90 kJ/mol). This likely results from the covering of ZrO₂ dissociation sites by a polytungstate monolayer, which may also act as secondary H₂ dissociation sites at higher temperatures.

H₂ dissociation has been shown to occur on ZrO₂ surfaces near room temperature to form ZrH⁻ and OH⁺ species.^{37,38} H₂ dissociation rates on several metal oxide supports were previously examined using similar temperature programmed D₂-OH exchange methods; these studies showed that both monoclinic and tetragonal ZrO₂ dissociate H₂ at lower temperatures than γ-Al₂O₃.³⁹ The inability of Al₂O₃ surfaces to provide the required hydrogen dissociation sites for the generation of reduced H-WO_x acid sites may account for the markedly different catalytic properties observed on WO_x-Al₂O₃ compared with WO_x-ZrO₂ for acid-catalyzed reactions aided by H₂.

If ZrO₂ sites on WO_x-ZrO₂ catalysts act as H₂ dissociation sites, the density of these sites and the rate constant (*k*) should decrease with increasing WO_x surface density as the ZrO₂ surface is covered by WO_x domains (Figure 8a). However, the calculated rate constants in Table 3 do not show any clear trends with WO_x surface density within experimental certainty.

Conclusions

The surface and acid properties of WO_x-ZrO₂ acid catalysts were characterized in the presence of H₂, and related to changes in the surface density and reducibility of WO_x species. NH₃ adsorption showed that acidic OH groups form on polytungstate domains with bridging W-O-W bonds. However, H₂ did not significantly affect the density of these Bronsted acid sites, indicating that these Bronsted acid sites are not responsible for the high rates observed for *o*-xylene isomerization in the presence of H₂ on WO_x-ZrO₂. Changes in H₂ chemisorption uptakes with WO_x surface density followed the same trend with WO_x surface density as *o*-xylene isomerization rates; both reached a maximum value at intermediate WO_x surface densities. The polytungstate domains prevalent at intermediate surface densities are both accessible and partially reducible, and are able to stabilize H^{δ+} Bronsted acid sites via redox processes on WO_x-ZrO₂. The density of H^{δ+} Bronsted acid sites formed from H₂ is very small on WO_x-ZrO₂, and their formation may be aided by H₂ dissociation on the ZrO₂ support.

Acknowledgment. Financial support for this work was obtained from the National Science Foundation (CTS-9510575). We acknowledge the use of *o*-xylene isomerization data obtained by Dr. David G. Barton, previously published in refs 17 and 19.

References and Notes

- (1) Tanabe, K.; Holderich, W. F. *Appl. Catal. A: Gen.* **1999**, *181*, 399–434.
- (2) Hino, M.; Arata, K. *J. Chem. Soc., Chem. Commun.* **1980**, 851–852.
- (3) Hsu, C. Y.; Heimbuch, C. R.; Armes, C. T.; Gates, B. C. *J. Chem. Soc., Chem. Commun.* **1992**, 1645.
- (4) Wan, K. T.; Khouw, C. B.; Davis, M. E. *J. Catal.* **1996**, *158*, 311–326.
- (5) Cheung, T.-K.; Gates, B. C. *Top. Catal.* **1998**, *6*, 41–47.
- (6) Adeeva, V.; de Haan, J. W.; Janchen, J.; Lei, G. D.; Schunemann, V.; van de Ven, L. J. M.; Sachtler, W. M. H.; van Santen, R. A. *J. Catal.* **1995**, *151*, 364–372.
- (7) Hino, M.; Arata, K. *J. Chem. Soc., Chem. Commun.* **1987**, 1259–1260.
- (8) Iglesia, E.; Barton, D. G.; Soled, S. L.; Misco, S.; Baumgartner, J. E.; Gates, W. E.; Fuentes, G. A.; Meitzner, G. D. *Stud. Surf. Sci. Catal.* **1996**, *101*, 533.
- (9) Chu, H. Y.; Rosynek, M. P.; Lundsford, J. H. *J. Catal.* **1998**, *178*, 352–362.
- (10) Hattori, H.; Shishido, T. *Catal. Surveys Jpn.* **1997**, *1*, 205–213.
- (11) Iglesia, E.; Soled, S. L.; Kramer, G. B. *J. Catal.* **1993**, *144*, 238–253.
- (12) Baertsch, C. D.; Wilson, R. D.; Barton, D. G.; Soled, S. L.; Iglesia, E. *Stud. Surf. Sci. Catal.* **2000**, *130*, 3225.
- (13) Wilson, R. D.; Barton, D. G.; Baertsch, C. D.; Iglesia, E. *J. Catal.* **2000**, *194*, 175–187.
- (14) Ebitani, K.; Konishi, J.; Hattori, H. *J. Catal.* **1991**, *130*, 257–267.
- (15) Santiesteban, J. G.; Vartuli, J. C.; Han, S.; Bastian, R. D.; Chang, C. D. *J. Catal.* **1997**, *168*, 431–441.
- (16) Scheithauer, M.; Cheung, T.-K.; Jentoft, R. E.; Grasselli, R. K.; Gates, B. C.; Knozinger, H. *J. Catal.* **1998**, *180*, 1–13.
- (17) Barton, D. G.; Soled, S. L.; Iglesia, E. *Top. Catal.* **1998**, *6*, 87–99.
- (18) Barton, D. G.; Shtein, M.; Wilson, R. D.; Soled, S. L.; Iglesia, E. *J. Phys. Chem.: B* **1999**, *103*, 630–640.
- (19) Barton, D. G.; Soled, S. L.; Meitzner, G. D.; Fuentes, G. A.; Iglesia, E. *J. Catal.* **1999**, *181*, 52–72.
- (20) Kubelka, P.; Munk, F. Z. *Technol. Phys.* **1931**, *12*, 593.
- (21) *Practical Sampling Techniques for Infrared Analysis*; Coleman, P. B., Ed.; CRC Press: Boca Raton, FL, 1993.
- (22) Ramis, G.; Cristiani, C.; Elmi, A.; Pierluigi, V. *J. Mol. Catal.* **1990**, *61*, 319–331.
- (23) Ramis, G.; Busca, G.; Cristiani, C.; Lietti, L.; Forzatti, P.; Bregani, F. *Langmuir* **1992**, *8*, 1744–1749.
- (24) Bachiller-Baeza, B.; Rodriguez-Ramos, I.; Guerrero-Ruiz, A. *Langmuir* **1998**, *14*, 3556–3564.
- (25) Scheithauer, M.; Grasselli, R. K.; Knozinger, H. *Langmuir* **1998**, *14*, 3019–3029.
- (26) Mapes, J. E.; Eischens, R. P. *J. Phys. Chem.* **1954**, *58*, 1059–1062.
- (27) Ramis, G.; Busca, G.; Bregani, F.; Forzatti, P. *Appl. Catal.* **1990**, *64*, 259–278.
- (28) Larsen, G.; Raghavan, S.; Marquez, M.; Lotero, E. *Catal. Lett.* **1996**, *37*, 57–62.
- (29) Yamaguchi, T.; Nakano, Y.; Tanabe, K. *Bull. Chem. Soc. Jpn.* **1978**, *51*, 2482–2487.
- (30) DeKock, R. L.; Gray, H. B. *Chemical Structure and Bonding*, 2nd ed.; University Science Books: Sausalito, CA, 1989.
- (31) Echterhoff, R.; Knozinger, E. *Surf. Sci.* **1990**, *230*, 237–244.
- (32) Dang, Z.; Anderson, B. G.; Amenomiya, Y.; Morow, B. A. *J. Phys. Chem.* **1995**, *99*, 14437–14443.
- (33) Soled, S. L.; McVicker, G. B.; Murrell, L. L.; Sherman, L. G.; Dispenziere, N. C.; Hsu, S. L.; Waldman, D. *J. Catal.* **1988**, *111*, 286–295.
- (34) Vaudagna, S. R.; Canavese, S. A.; Comelli, R. A.; Figoli, N. S. *Appl. Catal. A: Gen.* **1998**, *168*, 93–111.
- (35) Vaidyanathan, N.; Houalla, M.; Hercules, D. M. *Catal. Lett.* **1997**, *43*, 209.
- (36) Rajagopal, S.; Marzari, J.; Miranda, R. *J. Catal.* **1995**, *151*, 192–203.
- (37) Onishi, T.; Abe, H.; Maruya, K.; Domen, K. *J. Chem. Soc., Chem. Commun.* **1985**, 617–618.
- (38) Kondo, J.; Domen, K.; Maruya, K.; Onishi, T. *Chem. Phys. Lett.* **1992**, *188*, 443–445.
- (39) Martin, D.; Duprez, D. *J. Phys. Chem.: B* **1997**, *101*, 4428–4436.